JOC The Journal of Organic Chemistry

Article

pubs.acs.org/joc

Absolute Configuration and Conformation of Two Fráter–Seebach Alkylation Reaction Products by Film VCD and ECD Spectroscopic Analyses

Mohammad Reza Poopari, Zahra Dezhahang, Ke Shen, Lei Wang, Todd L. Lowary, and Yunjie Xu*

Department of Chemistry, University of Alberta, 11227 Saskatchewan Drive, Edmonton, Alberta T6G 2G2, Canada

Supporting Information

ABSTRACT: Two chiroptical spectroscopic techniques, namely, electronic and vibrational circular dichroism (ECD and VCD), as well as NMR spectroscopy have been utilized to determine the absolute configurations and geometries of two Fráter–Seebach alkylation reaction products with long hydrocarbon chains. The experimental studies have been complemented with density functional theory calculations. Strong characteristic bisignate VCD signatures in the carbonyl stretching region have been observed for both compounds in film state. Truncated models, i.e., without the long CH_2 chains, have been utilized to examine different hydrogen-bonding topologies between two monomeric moieties and to simulate the corresponding IR and VCD spectra of the dimers. In addition, the exciton coupling model has also been applied to the —C═O groups of the two monomeric moieties, which can be coupled through intermolecular hydrogen-bonding. On the basis of these simplified approaches, the absolute configurations of the compounds have been unambiguously assigned using VCD and ECD spectroscopy. Spectral simulations in the IR and UV–vis regions have also been carried out with the full dimers to validate the fitness of the truncated model. The study shows that the combination of the film VCD and ECD techniques is a relatively straightforward method to determine the absolution configurations of such synthetic compounds.

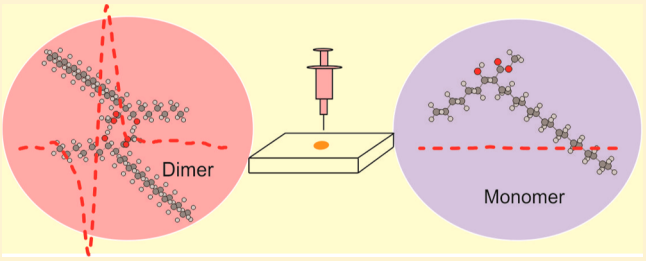

INTRODUCTION

The Fráter–Seebach alkylation[1,2] reaction is an efficient means for the diastereoselective introduction of α-substituents to chiral β-hydroxy esters using superbases such as lithium diisopropylamide (LDA) or lithium bis(trimethylsilyl)amide (LHMDS). In such reactions, both hydrocarbon groups, which are connected to the two stereogenic carbon centers of the β-hydroxy ester product (Figure 1), can be engineered as needed.[3] In the current study, two chiral β-hydroxy esters with different lengths of α-hydrocarbon chain substituents (**1** and **2**, Figure 1) have been synthesized by using the Fráter–Seebach alkylation reaction. Each product contains two stereogenic carbon centers where one is connected to an −OH group and the other one to an ester (−CO_2Me) group. In addition, a long hydrocarbon chain is attached to each stereogenic carbon center. The synthesis of **1** was reported before,[4,5] whereas that of **2** is reported here for the first time.

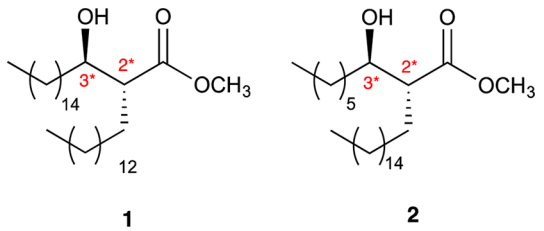

1 **2**

Figure 1. Chemical structure of **1** and **2**. The stereogenic centers are indicated with *.

These compounds are synthetic analogs of mycolic acids, lipids that are found in the cell wall of a number of actinomycete bacteria.[6] In particular, they are important constituents of cell wall arabinogalactan in the human pathogens *Mycobacterium tuberculosis* and *Mycobacterium leprae*, the causative agents of tuberculosis and leprosy, respectively.[7] The two compounds have been synthesized for use in the preparation of a library of glycolipids that will be used to probe the host immune response that occurs upon infection by mycobacteria.

One of the most important properties for further biological and other applications is the absolute configuration of the products. The three-dimensional spatial arrangement of a chiral molecular system can be determined by using different spectroscopic tools such as NMR spectroscopy, X-ray crystallography, electronic circular dichroism (ECD) spectroscopy, and vibrational CD (VCD) spectroscopy. Each method has its own pros and cons and also level of confidence in the absolute configuration assignment. While X-ray crystallography has been used extensively for this purpose, it is often tedious if not impossible to obtain the necessary single crystals for many

Received: October 24, 2014
Published: December 1, 2014

   dx.doi.org/10.1021/jo502438a | J. Org. Chem. 2015, 80, 428–437

synthetic products. VCD spectroscopy has been utilized successfully in recent years to determine absolute configurations and characterize chiroptical properties of synthetic compounds[8] and natural products.[9] In this study, we have applied both VCD and ECD spectroscopies, complemented with density functional theory (DFT) calculations, to determine the absolute configuration (AC) of these products and to characterize the associated hydrogen (H)-bonding interactions under film conditions. We have further discussed the benefits of using two complementary chiroptical spectroscopic tools to enhance the level of confidence in the AC assignments.[10] For comparison, the absolute configuration of the stereogenic carbinol carbon, i.e., 3* in Figure 1, has also been established by using an approach similar to the Mosher ester method[11] and complemented with the DFT calculations of NMR chemical shifts.

The VCD and ECD measurements have been carried out by using a cast film in the current study. There are a number of advantages associated with the cast film technique. One is that the resulting spectra have no contribution from the solvent molecules and no interference from the solvent molecules through H-bonding interactions or other intermolecular interactions. The latter greatly simplifies the necessary theoretical modeling for spectral interpretation. The other point is that the film measurements generally require less amount of sample compared to the solution measurements.[12] For example, Polavarapu and co-workers found that for L-phenylalanine and L-tryptophan, which have low solubility in water, the cast film technique is the method of choice.[13] Not only strong water interference could be eliminated to uncover amide I bands,[14] but also the signal-to-noise ratio of film-VCD spectra was enhanced noticeably compared to that obtained in solution.[15] More recently, the reversal of helical chirality of fibrils in dried film under different pH conditions was studied by Nafie and co-workers using VCD spectroscopy.[16] One known drawback of the cast film VCD technique is the possible formation of microcrystalline assemblies during film preparation, thus preventing artifact-free VCD spectra to be obtained. This, however, depends on specific solute and solvent properties and can be avoided by choosing an appropriate solvent or using the matrix-assisted film-VCD technique reported previously.[17] Experimental aspects of solid state VCD measurements were reviewed by Abbate and co-workers.[18] Furthermore, procedures for verifying if the system is free of such artifacts and for correcting such artifacts were reported before[19] and have utilized in the current study.

RESULTS AND DISCUSSION

1. Experimental IR and VCD Spectra in Film and in Solution. Figure 2 shows the experimental IR spectra of **1** in film and in $CDCl_3$ solvent. Clearly, the main IR features are similar in film and in solution, except the noticeable baseline elevation and band overlapping in the region below 1450 cm^{-1} in the solution measurement due to solvent interference. The film IR spectrum also shows two closely spaced bands at ~1720 cm^{-1} separated by ~12 cm^{-1}, while the corresponding feature in solution shows only one broad band at roughly the same position. The raw solution IR spectrum and the corresponding solvent IR spectrum are provided in Figure S1, Supporting Information. The corresponding VCD spectrum in solution, on the other hand, shows a poor signal-to-noise ratio, possibly a result of intermolecular interactions with $CDCl_3$.[20] Because of the limited amount of the synthetic sample, no further testing

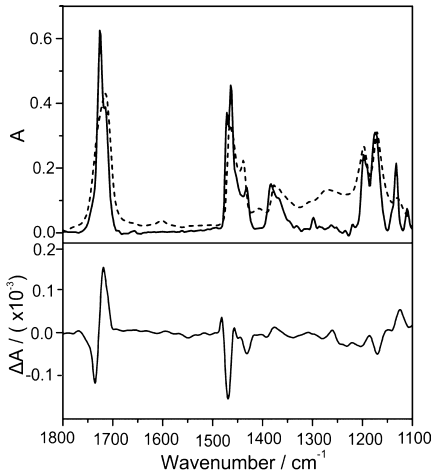

Figure 2. Experimental IR spectra of **1** in film (solid) and in $CDCl_3$ solution (dashed). The corresponding experimental VCD spectrum in film is shown at the bottom.

with other solvents was carried out. Rather, we focus on the experimental data obtained with the film method.

The observation of the two closely spaced IR bands in the —C═O stretching region in film may indicate the formation of a dimer. This is because the monomer of **1** features essentially only one type of intramolecular H-bond with the hydroxyl H atom pointing to the carbonyl O atom (Section 3). Furthermore, differences in the orientation of the hydrocarbon chains typically result in much smaller separation in the carbonyl region than that observed (Section 3). The clear evidence for the formation of a dimer comes from the greatly enhanced +/− bisignated VCD couplet in the same region, going from low to high wavenumber. Such noticeably enhanced VCD signatures are common for two strongly coupled —C═O oscillators.[21−23] On the other hand, one would generally expect low VCD intensity in the carbonyl stretching region if the two oscillators are not coupled, for example, from conformers due to different hydrocarbon chain orientations (see Section 3).

2. NMR Spectroscopic and DFT Determination of Chirality at the Carbinol C Atom. There are two stereogenic centers in these two products: one is at the carbinol C atom whose chirality was set by an enantioselective reduction of a ketone using a chiral catalyst and the other during the alkylation reaction (see Experimental Section). In this section, we utilized an approach analogous to the Mosher ester analysis[11] for the determination of the absolute configuration of the stereogenic carbinol carbon atom. Since α-methoxy-α-trifluoromethylphenylacetic acid (MTPA−OH), also known as Mosher's acid, is rather expensive, we chose a cheaper chiral acid, i.e., (*S*)-(+)-*O*-acetylmandelic acid, as our NMR shift agent. Briefly, **3**, the product of the above enantioselective reduction of a ketone and a precursor for **1**, was reacted with (*S*)-(+)-*O*-acetylmandelic acid, as shown in Scheme 1. Since **3** was produced with 93% ee, we expected to obtain two diastereomeric esters with (2*R*,5*S*) and (2*S*,5*S*) absolute configurations. The resulting ester ^{1}H NMR spectroscopic experiments show two well resolved peaks at 3.64 and 3.37 ppm with the latter having much less intensity, arising from the methyl group of the methyl ester. Generally speaking, because of the different orientation of the phenyl group in these two diastereomeric esters shown in Figure 3, one may speculate that

dx.doi.org/10.1021/jo502438a | J. Org. Chem. 2015, 80, 428−437

Scheme 1. Production of a Mosher Ester Analogue for the NMR Spectroscopic Determination of the Absolute Configuration at the Carbinol C of 3

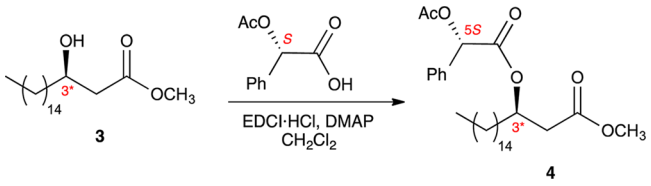

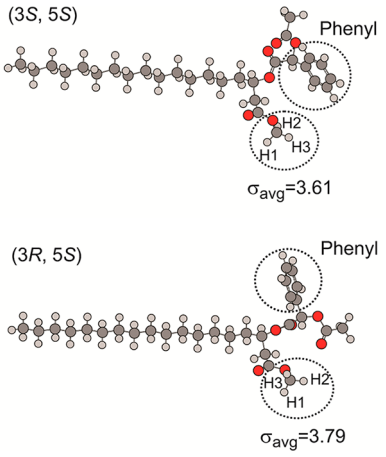

Figure 3. Optimized geometries of the two diastereomeric esters (3*S*,5*S*) and (3*R*,5*S*) and the corresponding NMR shifts of the methyl protons predicted at the 6-311++G(d,p)//6-31+G(d) level. The first and second chiral labels refer to the chirality of the carbinol carbon and the acid used, respectively. Note that in (3*S*,5*S*), the methyl protons are better shielded by the aromatic group than in (3*R*,5*S*), as highlighted with dotted lines.

the methyl protons in the (2*S*,5*S*) ester are more shielded and therefore move upfield in its NMR spectrum. To validate this assumption, the corresponding DFT calculations at the 6-311++G(d,p)//6-31+G(d) was carried out. The ($\delta_{RS} - \delta_{SS}$) NMR shift value was predicted to be +0.18 ppm, in good agreement with the experimental +0.27 nm. In calculating these NMR shifts, we have adopted the linear scaling model reported by Rablen et al.[24] From this combined experimental and theoretical approach, we deduced that the chirality at the carbinol C of the **1** and **2** is *R* for the major product.

3. Absolute Configuration of 1 and 2 from Chiroptical Spectroscopy with Simplified Models. *Truncated Models.* For both **1** and **2**, the −OH and $-CO_2Me$ groups can in principle adopt two H-bonding topologies, i.e., —OH···O═C or —OH···OMe intramolecular H-bonds. It is well documented that the —OH···O═C H-bonding topology is strongly preferred.[25,26] The more subtle conformations related to the long hydrocarbon chains will be addressed in Section 4.

In order to determine the absolute configurations of the **1** and **2** from chiroptical measurements in film, we need to consider the H-bonded dimers alluded to in Section 1. First, the experimental IR and VCD spectra of both **1** and **2** with different alkyl chains show somewhat similar features in the fingerprint region (vide infra). Second, the most prominent VCD features observed are in the carbonyl stretching region, whereas the vibrational modes of the alkyl chains in the fingerprint region are generally below 1500 cm^{-1}. We therefore decided to first utilize the truncated models where the long alkyl chains are replaced with the methyl groups to reduce computational cost. Such simplified approach was reported before for complex systems with a long hydrocarbon chain or formed H-bonded dimers.[27]

Two intermolecular H-bonding models are proposed in Figure 4. In Model_I, the two O═C groups act as the proton acceptors and the −OH groups as the H-donors. In Model_II,

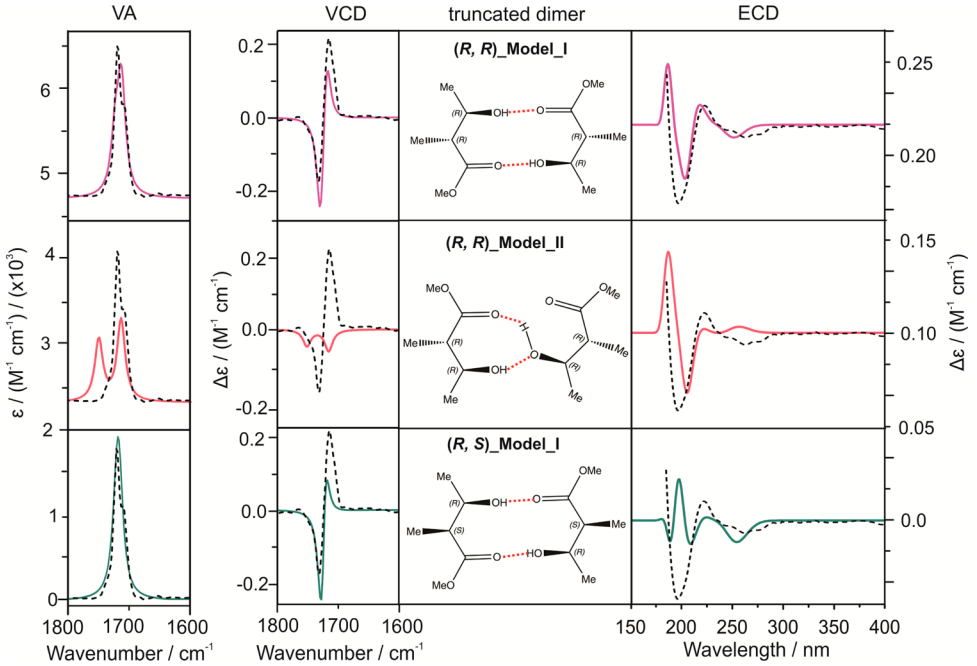

Figure 4. Calculated VA and VCD spectra (left) in the carbonyl stretching region and ECD spectra (right) of the truncated dimers. The truncated models used are provided in the middle. For clarity, only experimental VA and VCD data (dotted line) of **1** and ECD data of **2** are shown for comparison. The vertical units are those of the calculated ones.

dx.doi.org/10.1021/jo502438a | *J. Org. Chem.* 2015, 80, 428−437

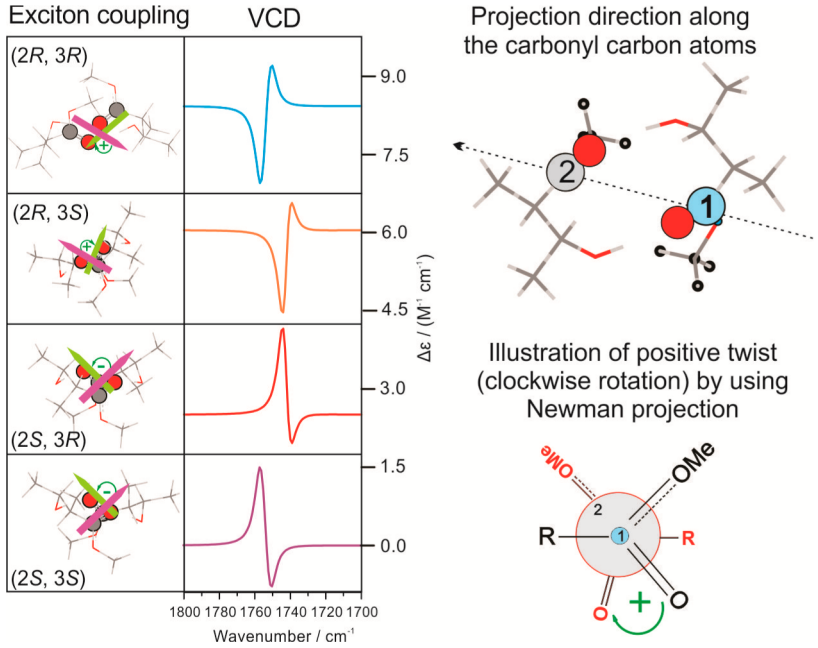

Figure 5. Illustration of the exciton coupling phenomenon of the two chromophoric carbonyl moieties in Model_I.

one hydroxyl group is inserted into the existing intramolecular H-bond of the other molecule and acts both as the H-donor and acceptor. The simulated IR and VCD spectra of Model_I and II of the truncated (2*R*,3*R*) and (2*S*,3*R*) products in the 1800 to 1700 cm^{-1} region. The corresponding results of (2*S*,3*S*) and (2*R*,3*S*) are not shown since (2*S*,3*S*) and (2*R*,3*S*) give the same IR and the mirror-imaged VCD spectra as (2*R*,3*R*) and (2*S*,3*R*), respectively. In Model_I where the two —C═O groups are involved in the intermolecular H-bonded ring, the calculated VCD features exhibit greatly enhanced intensity with the +/− bisignate couplet from low to high wavenumber for both (*R*,*R*) and (*R*,*S*) isomers. For Model_II, since one —C═O group is not involved in the intermolecular H-bonding interaction, its IR band appears blue-shifted relative to the one which is involved in the intermolecular H-bond. The said IR band is also blue-shifted with respective the IR bands of the two —C═O groups in Model_I, which are both involved in the H-bonds. Furthermore, in Model_II, the two —C═O groups are not coupled oscillators. Their motions clearly appear to be independent of each other in GaussView.[28] As a result, the VCD features in this region change from the intense +/− bisignate pattern in Model_I to two weak negative bands, which are well separated in wavenumber in Model_II.

It is interesting to note that both the (2*R*,3*R*) and (2*S*,3*R*) isomers in Model_I generate similar VCD features in the carbonyl stretching region. This is somewhat unexpected since the carbinol C is further away from the —C═O group than the second chiral C atom which is directly connected to the $-CO_2Me$ group. One may intuitively expect that the chirality of C connected to the ester group would have a greater influence on the VCD features at the carbonyl stretching region than the carbinol chirality. In this case, such a "common-sense" prediction has not worked. A closer examination of the related diastereomeric structures reveal that the carbonyl groups in the (2*S*,3*R*) isomer need to twist differently compared to those in the (2*R*,3*R*) isomer in order to form the intermolecular H-bonds. Indeed, researchers in the chiroptical field have become increasingly aware of the effects of conformational or structural twists on chiroptical spectral features, in addition to the permanent chirality of the system.[29,30] In this particular case one can picture a structural arrangement that generates a positive twist for the two coupled —C═O groups using the exciton coupling model discussed below. Clearly, Model_I with the (2*R*,3*R*) and (2*S*,3*R*) isomers are both consistent with the experimental VCD data, while the carbonyl VCD features of Model_II deviate noticeably from the experiment. Therefore, the VCD study indicates that chirality at the carbinol C atom is *R*, consistent with the NMR spectroscopic result. However, one cannot tell if the compound is of (2*R*,3*R*) or (2*S*,3*R*) with only the experimental carbonyl VCD features.

To complement the VCD study, we have also carried out ECD spectral simulations of the two aforementioned models and the related diastereomers. The resulting calculated ECD spectra are also summarized in Figure 4. Experimentally, ECD spectra of both **1** and **2** consist of a broad and shallow negative, a positive, and a strong negative band, going from long to short wavelengths. For simplicity, only the ECD spectrum of **2** is shown in Figure 4, while that of **1** is provided in the next section. As one can see, the experimental ECD data are again well-captured by Model_I with the (2*R*,3*R*) isomer. Furthermore, the simulated ECD features of Model_I with the (2*S*,3*R*) isomer are considerably different that those of the (2*R*,3*R*) isomer. Therefore, ECD spectral features also allow one to identify the chirality at both stereogenic carbons. The combined ECD and VCD approach is desirable. The VCD features provide a clear indication of the formation of the H-bonded dimer and the preferred H-bonding model utilized, thus greatly reducing the amount of structural search needed, while the ECD features provide a clear discrimination among the diastereomers proposed. Therefore, the combined ECD and VCD spectroscopic approach enables one to determine the chirality of the stereogenic centers of these two synthetic compounds independently of the NMR spectroscopic data.

Exciton Coupling Model. The exciton coupling model has been used broadly and successfully to interpret ECD spectral features since its development by Harada and Nakanishi.[31] One

dx.doi.org/10.1021/jo502438a | *J. Org. Chem.* 2015, 80, 428−437

attractive feature is that it is easy to use, with little computational demand. More recently, Monde et al. explored the application of this method for interpreting VCD spectral features.[32] The —C═O stretching modes are well-suited for the VCD exciton coupling approach because they are well-localized and often well separated from other modes, and their related electric transition moments are essentially parallel to the C═O bond. We have therefore tested the validity of such a simple and useful approach on these two synthetic compounds here.

Both **1** and **2** show a bisignate VCD signal at ~1720 cm^{-1}. Such spectral features imply the presence of two electric transition moments, which can interact through space, thus causing the split-type bisignate VCD signals. The absorbing chromophores can either be identical or not. More importantly, they do not necessarily need to exist in the same molecule to start with. Rather, in the current case, dimerization through intermolecular H-bonding interaction is enough to bring the two chromophores close enough to couple and to cause the bisignate VCD signatures.[33] If the two chromophoric sites are oriented in a positive twist with respect to each other, i.e., clockwise rotation, looking down from the closest electric transition moment to the one further away, it produces +/− couplet signals from low to high wavenumber (see Figure 5). The opposite coupling features are generated if the two transition moments are in a negative twist arrangement, i.e., counterclockwise rotation. As can be seen in Figure 5, the two —C═O bonds are in a positive twist in Model_I with the (2*R*,3*R*) monomers and therefore capture the experimental signatures correctly, while the two are in a negative twist with the (2*S*,3*S*) monomers. Furthermore, the dimer with the (2*S*,3*R*) monomers also provides a positive twist, consistent with the truncated models discussed before.

While the exciton VCD method works well for the two —C═O bonds in Model_I where both are involved in the same intermolecular H-bonded ring, its application to the two —C═O bonds in Model_II is less obvious. Although geometrically these two —C═O chromophores are in a negative twist in Model_II with the (*R*,*R*) isomer (see Figure S2, Supporting Information), the corresponding VCD signatures in the —C═O stretching region emerge as two weak negative bands rather than an intense bisignate couplet. It appears that these two chromospheres do not have any strong coupling with each other. This was already alluded to in the discussion of the truncated Model_II (Figure 5). In Model_II, the stretching motions of the two —C═O groups show essentially no synchronization at all, i.e., no symmetric and antisymmetric characters. Rather, they are independent of each other and therefore exciton coupling does not apply here.

4. Spectral Simulations with Full 1 and 2 Monomers and Dimers. The simplified models such as the truncated model and exciton coupling method work well to provide the absolute configuration assignments from the experimental spectra. However, we thought it important to extend the calculations to include full geometries of both monomers and dimers of **1** and **2** to test the validity of the truncated model and to examine what additional information can be extracted from the experimental data. For the monomer of **1**, our preliminary molecular mechanics simulation shows a large number of conformers with bends at different positions of the long hydrocarbon chains. The most stable conformers sampled are provided in Figure S3, Supporting Information, together with their corresponding IR and VCD spectra. There is only one dominant conformer that has the —OH···O(═C) H-bond and all CH_2 groups in the *trans* arrangement, i.e., both alkyl groups extended. The latter finding is consistent with previous experimental and theoretical studies, which showed that the all *trans* conformation is by far the dominant one for the shorter chains such as those considered here.[34]

For the full dimer geometry, we utilized the dominant all *trans* monomeric conformer and the intermolecular H-bonding topology of Model_I. Dimers containing bended hydrocarbon chains are much less stable than that with all *trans* hydrocarbon chains. So are those with Model_II binding topology. Therefore, these much less stable conformers are not considered further here. The dominant monomeric and dimeric geometries are summarized in Figure 6 for both **1** and **2**. We

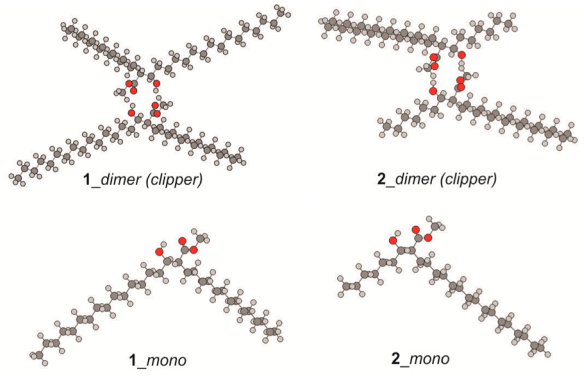

Figure 6. Dominant monomeric and dimeric structures of **1** and **2**.

have also tested the inclusion of dispersion correction in our calculation. This resulted in a geometry in which the hydrocarbon chains are bunched together rather than extended (see Figure S4, Supporting Information). This is likely due to an overcorrection of the dispersion interaction.[35] The resulting IR and VCD spectra of the dimer of **1** (*bunched*) are compared with the corresponding experimental data in Figure S5, Supporting Information. The agreement achieved with the dispersion correction is somewhat worse compared to the standard DFT calculation, and we therefore left out the dispersion correction in the remainder of the paper.

Figure 7 shows the comparison of the experimental and theoretical VA and VCD spectra of the monomer and dimer of **1**. As can be seen, the simulated IR spectrum of the **1**_*dimer* (*clipper*) captures essentially all the important IR bands observed in this region, although the relative intensities of some IR bands are not reproduced precisely. For example, the triplet IR bands observed in the 1500−1400 cm^{-1} region were observed with higher relative intensity than predicted. The agreement between the simulated IR spectrum of the **1** monomer and the experimental data is considerably worse. For the corresponding VCD spectra, the prominent +/− couplet from low to high wavenumber observed in the carbonyl stretching region is well reproduced by the dimer, but not at all by the monomer. This is consistent with the truncated model and exciton coupling model presented above. The +/−/+ triplet features observed experimentally in the 1500−1400 cm^{-1} region are also reproduced theoretically, although the predicted intensity is lower than the experimental one, as in the case of the corresponding IR bands. Making detailed assignments in the low wavenumber region is challenging because the vibrational modes associated with the hydrocarbon chains

dx.doi.org/10.1021/jo502438a | J. Org. Chem. 2015, 80, 428−437

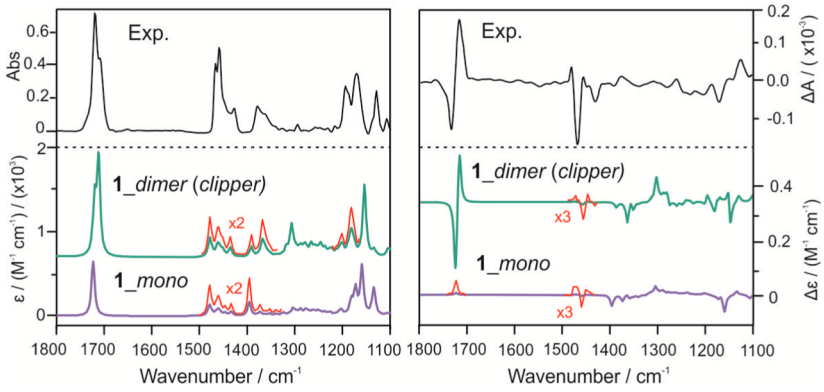

Figure 7. Comparison of the experimental IR (left) and VCD (right) spectra with the corresponding simulated spectra of the dominant monomer and dimer of **1** at the B3LYP/cc-pVTZ level of theory.

such as scissoring, wagging, twisting motions of CH_2 groups, bending motions of $-CH_3$ groups (both terminal methyl of the hydrocarbon chains and the $-CO_2Me$ groups), and bending modes of $-C_\alpha H$ and $-OH$ groups overlap severely. Overall, **1**_*dimer* (*clipper*) provides satisfactory agreement with the experiment, while its monomer does not.

For the sake of completeness, simulations of the UV−vis and ECD spectra of both monomer and dimer of **1** were carried out. Figure 8 shows the comparison of the experimental and theoretical ECD spectra of the monomer and dimer of **1**, as well as the corresponding UV−vis spectra. In the calculated spectra, the monomer exhibits two bands centered at ∼170 and 205 nm, while the dimer shows an intense broad UV−vis peak at ∼210 nm and a low-intensity one at ∼275 nm, which are bathochromic shifted from those of the monomer due to intermolecular H-bonding interactions. The experimental UV−vis spectrum consists of a very broad band. As a result, one cannot differentiate between the monomer or dimer preference using the UV−vis spectrum. The experimental ECD spectrum consists of several Cotton bands with the −/+/+/− trend from long to short wavelengths. These unique spectral features are well reproduced by the simulated ECD spectrum of the dimer. To guide the eye, the experimental bands are labeled with numbers 1 to 4, while the corresponding calculated bands are labeled with 1′ to 4′. It is also clear that the monomer does not reproduce the experimental ECD data.

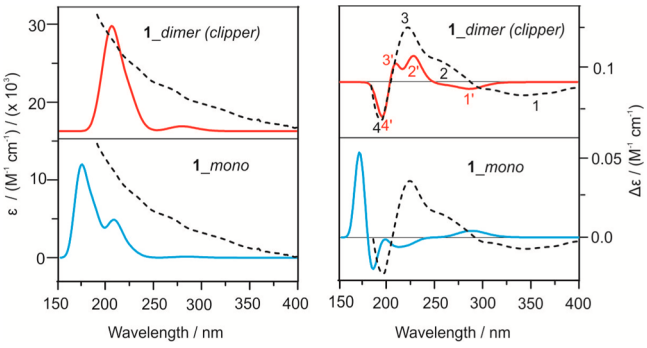

Figure 8. Experimental (dotted-line) UV−vis (left) and ECD (right) spectra are compared with the corresponding simulated (color solid-line) spectra of the dominant monomer and dimer of **1** at the B3LYP/6-31G(d,p) level of theory. The vertical units used are for the calculated ones. The experimental and the corresponding calculated ECD features of the dimer are marked with Arabic numbers 1−4 and 1′−4′, respectively.

The same calculation procedure has also been repeated for the monomer and dimer of **2**. Figure 9 shows the comparison of the experimental and theoretical VA and VCD spectra of **2**. The positions of almost all the observed IR bands are well reproduced by the simulated IR spectrum of the dimer of **2**, including the two closely spaced bands in the carbonyl stretching region. The intensity of some IR bands are not as well captured as their positions. For example, the triplet at the 1500−1400 cm^{-1} region was predicted to be less intense than observed, similar to the case of **1**. As can be seen from Figure 9, the corresponding observed VCD spectral features can be satisfactorily assigned based on the predicted VCD spectrum of the dimer of **2**. Not only the intense bisignate carbonyl VCD stretching bands due to the dimer are correctly captured, but also most of the VCD features in the lower wavenumber region. For example, the +/−/+ VCD features mentioned above are well reproduced by using the dimer but not by the monomer of **2**. Also, the +/+/−/− features from low to high cm^{-1} in the 1125−1100 cm^{-1} region are consistent with the dimeric structure of **2**.

Figure 10 compares the experimental UV−vis and ECD spectra with the corresponding simulated spectra of the monomer and dimer of **2**. As one can see, the simulated UV−vis and ECD spectra of the **2** dimeric *clipper* structure agree well with the corresponding experimental ones. For example, the −/+/− ECD features from long to short wavelength are well reproduced by the calculation. Overall, the dimeric *clipper* structure fulfills the experimental observation, allowing one to assign confidently the absolute configuration and dimeric *clipper* structure to the sample. The better agreement for **2** compared to **1** may perhaps be due to the fact that **2** contains one noticeably shorter hydrocarbon chain and thus less severe overlaps in the low wavenumber region.

Finally, we compared the simulated spectra using the full dimer geometries for these two compounds with the truncated Model_I. The experimental UV−vis spectra observed for both **1** and **2** are very broad, with no noticeable difference. The main experimental ECD features observed are also quite similar for both compounds, although the two positive ECD bands are better resolved for **1** than **2**. The simulated UV−vis and ECD spectra also appear similar for the **1**_*dimer* (*clipper*) versus the **2**_*dimer* (*clipper*). Furthermore, it is satisfying to note that the ECD simulations also capture the subtle differences in the

dx.doi.org/10.1021/jo502438a | J. Org. Chem. 2015, 80, 428−437

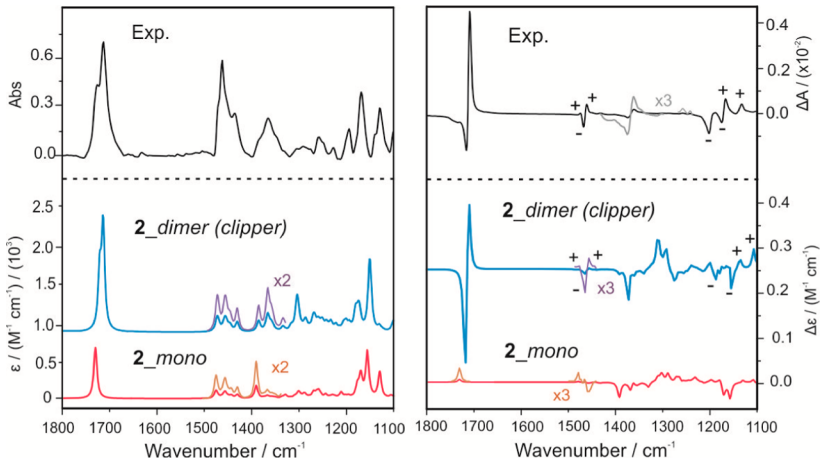

Figure 9. Comparison of the experimental IR (top) and VCD (bottom) spectra with the corresponding simulated spectra of the dominant monomer and dimer of **2** at the B3LYP/cc-pVTZ level of theory.

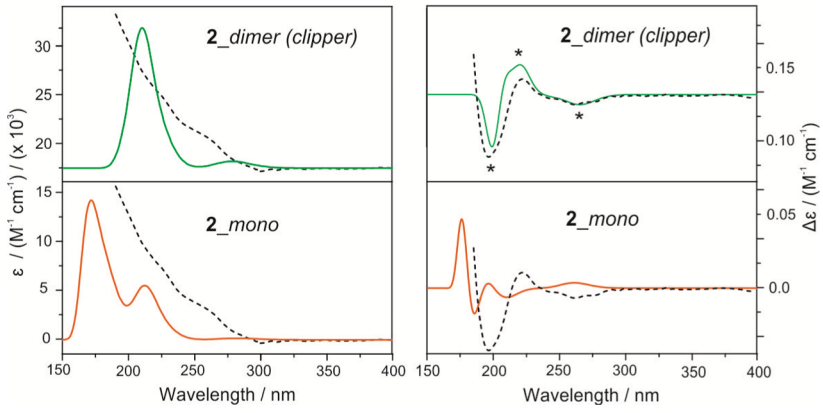

Figure 10. Experimental (dotted-line) and theoretical (colored solid-line) UV (left) and ECD (right) spectral comparison of the monomer and dimer structures of **2** at the B3LYP/6-31G(d,p) level of theory.

experimental ECD features of the **1** and **2** samples due to the length of the hydrocarbon side chains, although the length generally does not affect the electronic transitions and the corresponding ECD features significantly. This is essentially the reason for the success of the simplified truncated model. Since the IR and VCD spectra have a much narrower bandwidth and contain some vibrational modes directly related to the hydrocarbon chains in the fingerprint region, we compared the simulated IR and VCD spectra of **1**_*dimer* (*clipper*) and **2**_*dimer* (*clipper*) with those of the truncated Model_I in Figure S6, Supporting Information. In this fingerprint region, the IR spectra of all three systems look very much the same, while there are some obvious differences for the corresponding VCD spectra in the region below 1500 cm^{-1}. In particular, Model_I exhibits much different VCD features in the region below 1400 cm^{-1} from those of **1**_*dimer* (*clipper*) and **2**_*dimer* (*clipper*). This potentially means that some details about the hydrocarbon chains may be extracted from the VCD features in this region. Unfortunately, because of the severe overlapping of the bands in this region, it is currently very challenging to capture the VCD features *exactly* right in order to extract detailed structural information related to the hydrocarbon chains.

CONCLUSIONS

We have applied ECD and VCD spectroscopy, together with DFT calculations, to determine the absolute configurations and geometries of two Fráter−Seebach alkylation reaction products with long hydrocarbon chains to be (2*R*,3*R*) with extended all *trans* hydrocarbon chains. The strongly enhanced carbonyl stretching VCD features indicate that the compounds in the film state exist predominantly as H-bonded dimers. Two simplified models, i.e., the truncated model and the exciton coupling model, have also been utilized and tested against the calculations performed for the full dimers. It appears that these simplified models are sufficient to allow extraction of chirality information on the systems and to identify the main H-bonding interaction. We have also carried out an NMR spectroscopic study, complemented with DFT calculations, to determine the chirality of the carbinol carbon. Consistent results have been obtained with NMR spectroscopy and chiroptical spectroscopy. Overall, the study shows that the combination of the film VCD and ECD techniques is a relatively straightforward method to determine the absolution configurations of such synthetic compounds in film.

EXPERIMENTAL SECTION

IR and VCD Measurements. Compounds **1** and **2** were dissolved either in chloroform or acetone and a few drops of the resulting solution were placed on an CaF_2 window and let to dry at room

dx.doi.org/10.1021/jo502438a | J. Org. Chem. 2015, 80, 428−437

temperature. IR and VCD spectra were recorded using a Fourier transform IR spectrometer equipped with a VCD module. The concentration and film thickness were optimized so that the absorption coefficients of the IR bands of interest are in the range of 0.2−0.9. The spectral ranges of 1800−1100 cm^{-1} were selected for the purpose of this paper. All IR and VCD spectra were obtained with a resolution of 4 cm^{-1} and with a total measurement time of 3 h (3 × 1 h). The final reported VCD spectra were baseline corrected using the background spectra subtraction. A sample holder which can be rotated freely from 0° to 360° was constructed. The cast film CaF_2 window was mounted on the rotatable holder. The VCD spectra were found to be essentially the same with angles at 0°, 45° and 90°, confirming that the samples have no noticeable anisotropy.

UV−Vis and ECD Measurements. The UV−vis spectra of the samples in film were collected using a Spectrophotometer. The thickness of the cast film was optimized to have the UV−vis absorbance in the range of 0.2−0.9. Thereafter, the ECD spectra were collected using an circular dichroism spectrometer. The final ECD spectra were background-corrected.

Theoretical Modeling. The Gaussian 09[36] suite of programs has been used for all geometry optimization and harmonic vibrational frequencies calculations, as well as the IR and VCD intensities predictions. DFT[37] calculations were performed with the Becke, three-parameter, Lee−Yang−Parr (B3LYP)[38] hybrid functional and the augmented correlation-consistent triple-ζ basis sets, i.e., cc-pVTZ,[39] for final conformational calculations and spectral simulations. A factor of 0.98 was used for the frequency scaling. A Lorentzian line shape with a half-width at half-height (HWHH) of 4 cm^{-1} was used for the simulations of IR and VCD spectra.

UV−vis and ECD spectral simulations were carried out using the time dependent-DFT (TD-DFT) approach and the 6-31G(d,p) basis set. The basis set employed offers a good compromise between accuracy and computational expense. We have added an extra polarization p-function to the double-ζ 6-31G(d) basis set which is considered to be the minimal basis set recommended for optical spectral simulations.[40] UV−vis and ECD calculations for **1** were also done with 6-31+G(d) for comparison (see Figure S7, Supporting Information). The UV−vis spectra have been simulated with the first 100 electronic excited states. A Gaussian line shape with a half-width at half-height (HWHH) of 0.33 eV was used for the simulations of UV−vis and ECD spectra.

For the initial conformational search of **1** and **2**, we have employed the Spartan program.[41] About 1000 conformers were predicted by using either the universal force field (UFF) molecular mechanics (MM) or semiempirical AM1 method[42] and the "conformer distribution" option implemented in the Spartan program. About 100 most stable conformers were kept for further analyses and similar conformers were identified with the MM and AM1 methods. Four conformers were deemed relevant at room temperature with their relative energy within ∼20 kJ/mol. These most stable conformers were reoptimized with the DFT approach described above and only one dominant structure was identified. See the Results and Discussion section for more information.

Synthesis. *General Methods.* All reagents were purchased from commercial sources and were used without further purification unless noted. All reactions were carried out under a positive pressure of argon or nitrogen at room temperature unless specified and were monitored by TLC on silica gel 60-F_{254} (0.25 mm). Visualization of the reaction components was achieved using UV fluorescence (254 nm) and/or by charring with acidified anisaldehyde solution in ethanol. Organic solvents were evaporated under reduced pressure and the products were purified by column chromatography on silica gel (230−400 mesh). Optical rotations were measured in a microcell (10 cm, 1 mL) at ambient temperature and are in units of degree·mL/(g·dm). ^1H NMR spectra were recorded at 500 MHz and chemical shifts are referenced to residual $CHCl_3$ (7.26 ppm, $CDCl_3$). ^{13}C NMR spectra were recorded at 125 MHz and chemical shifts are referenced to $CDCl_3$ (77.0 ppm). Reported splitting patterns are abbreviated as s = singlet, d = doublet, t = triplet, m = multiplet, br = broad, app = apparent. ESI-TOF/MS spectra were recorded on samples suspended in THF or CH_3OH and added NaCl.

(2R,3R)-Methyl-3-hydroxy-2-tetradecyloctadecanoate (1).[4] A solution of lithium diisopropylamine (8 mL) prepared from *n*-BuLi (2.5 M hexane solution, 2.64 mL, 6.6 mmol) and diisopropylamine (0.93 mL, 6.6 mmol) was cooled to −78 °C, and the β-hydroxy ester **3**[4] (0.691 g, 2.2 mmol) was added as a solution in THF (2 mL). After 1 h at −45 °C, 1-iodododecane (1.43 g, 4.4 mmol) and HMPA (0.76 mL, 4.4 mmol) were added via a syringe. The mixture was stirred at −45 °C for 3 h then warmed slowly to −20 °C overnight. The mixture was treated with saturated NH_4Cl and extracted with ether. The ether layer was washed with brine, dried over $MgSO_4$ and concentrated. The crude product was purified by column chromatography (hexane−EtOAc, 10:1) to give **1** (0.44 g, 40%) as a white solid (Scheme 2): R_f = 0.67 (hexane−EtOAc, 4:1); $[\alpha]_D$ +4.8 (*c* 0.7, $CHCl_3$); ^1H NMR (500 MHz; $CDCl_3$) δ 3.71 (s, 3H), 3.68−3.62 (m, 1H), 2.43 (dt, 1H, *J* = 9.1, 5.3 Hz), 2.39 (d, 1H, *J* = 8.3 Hz), 1.73−1.25 (m, 54H), 0.88 (t, 6H, *J* = 7.0 Hz); ^{13}C NMR (125 MHz; $CDCl_3$) δ 176.2, 72.3, 51.4, 51.0, 35.7, 31.9, 29.68, 29.67, 29.65, 29.61, 29.58, 29.56, 29.55, 29.53, 29.49, 29.41, 29.35, 27.4, 25.7, 22.7, 14.1; HR ESIMS *m/z* $[M + Na]^+$ Calcd for $C_{33}H_{66}O_3Na$ 533.4903, found 533.4904.

Scheme 2. Synthetic Route for 1

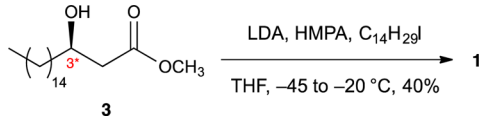

(R)-Methyl-2-((R)-1-hydroxyheptyl)octadecanoate (2). A solution of lithium diisopropylamine (5 mL) prepared from *n*-BuLi (1.6 M hexane solution, 2.5 mL, 4 mmol) and diisopropylamine (0.56 mL, 4 mmol) was cooled to −78 °C, and the β-hydroxy ester **5**[5] (0.37 g, 2 mmol, mixture of stereoisomers 50% ee) was added as a solution in THF (2 mL). After 1 h at −45 °C, 1-iodododecane (1.76 g, 2.5 mmol) and HMPA (0.52 mL, 1.5 mmol) were added via a syringe. The mixture was stirred at −45 °C for 5 h then warmed slowly to −20 °C overnight. The mixture was treated with saturated NH_4Cl and extracted with ether. The ether layer was washed with brine, dried over $MgSO_4$ and concentrated. The crude product was purified by column chromatography (hexane−EtOAc, 10:1) to give **2** (0.173 g, 21%, 50% ee) as a white solid (Scheme 3): R_f = 0.69 (hexane−EtOAc, 4:1); $[\alpha]_D$ +4.3 (*c* 0.6, $CHCl_3$); ^1H NMR (500 MHz; $CDCl_3$) δ 3.73 (s, 3H), 3.70−3.65 (m, 1H), 2.46 (dt, 1H, *J* = 9.2, 5.3 Hz), 2.42 (d, 1H, *J* = 8.3 Hz), 1.75−1.27 (m, 40H), 0.90 (t, 6H, *J* = 6.9 Hz); ^{13}C NMR (125 MHz; $CDCl_3$) δ 176.2, 72.3, 51.5, 51.0, 35.7, 31.94, 31.78, 29.71, 29.70, 29.67, 29.66, 29.64, 29.58, 29.51, 29.44, 29.37, 29.22, 27.4, 25.7, 22.70, 22.61, 14.13, 14.08; HR ESIMS *m/z* $[M + Na]^+$ Calcd for $C_{26}H_{52}O_3Na$ 435.3797, found 435.3809.

Scheme 3. Synthetic Route for 2

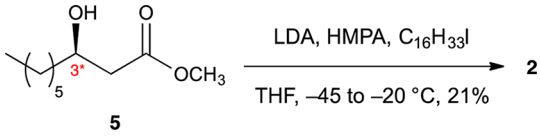

(S)-(+)-O-Acetylmandelic ester 4. To a stirred solution of β-hydroxy ester **3**[4] (62.9 mg, 0.2 mmol) and (*S*)-(+)-*O*-acetylmandelic acid (58.3 mg, 0.3 mmol) in CH_2Cl_2 (4 mL) was added EDCI·HCl (76.7 mg, 0.4 mmol) at 0 °C and the mixture was stirred for 1 min. Subsequently, DMAP (2.4 mg, 0.02 mmol) was added, and the mixture was stirred for an additional 30 min at the same temperature. The resulting mixture was diluted with CH_2Cl_2 (6 mL), and was washed with brine. The organic layer was dried over anhydrous Na_2SO_4 and concentrated. Then the resulting crude product was purified by column chromatography (hexane−EtOAc, 8:1) to give the **4** (93.1 mg, 17.8 mmol, 95%) as a white solid: R_f = 0.4 (hexane−

dx.doi.org/10.1021/jo502438a | J. Org. Chem. 2015, 80, 428−437

EtOAc, 4:1); ^{1}H NMR (400 MHz; $CDCl_3$) δ 7.46−7.44 (m, 2H), 7.39−7.35 (m, 3H), 5.86 (s, 3H), 5.25−5.22 (m, 1H), 3.63 (s, 1H), 2.64 (dd, 1H, J = 15.6, 7.6 Hz), 2.52 (dd, 1H, J = 15.6, 5.6 Hz), 2.17 (s, 1H), 1.50−1.44 (m, 2H), 1.26−0.95 (m, 26H), 0.88 (t, 3H, J = 7.0); ^{13}C NMR (100 MHz; $CDCl_3$) δ 170.0, 169.7, 167.8, 133.5, 128.8, 128.3, 127.2, 74.2, 71.5, 51.4, 38.7, 33.4, 31.5, 29.3, 29.2, 29.0, 28.9, 28.7, 24.1, 22.3, 20.2, 13.7; HR ESIMS m/z $[M + Na]^+$ Calcd for $C_{29}H_{46}O_6Na$: 513.3187, found 513.3177.

■ ASSOCIATED CONTENT

Supporting Information

Raw IR spectra of **1** and $CDCl_3$ solvent; Exciton coupling of (*R*,*R*)_Model_II; Conformers of **1** and their IR and VCD spectra; The structure of **1**_*dimer* (*bunched*) and its IR and VCD spectra; IR and VCD spectra of full **1** and **2** *dimer* and of the truncated Model_I. ^{1}H and ^{13}C NMR spectra of **1**, **2** and **4**. This material is available free of charge via the Internet at http://pubs.acs.org.

■ AUTHOR INFORMATION

Corresponding Author

*E-mail: yunjie.xu@ualberta.ca.

Notes

The authors declare no competing financial interest.

■ ACKNOWLEDGMENTS

This research was funded by the University of Alberta, the Natural Sciences and Engineering Research Council of Canada and the Alberta Glycomics Centre. We also gratefully acknowledge access to the computing facilities provided by the Academic Information and Communication Technology group at the University of Alberta and by the Western Canada Research Grid (Westgrid). Y.X. holds a senior Canada Research Chair in Chirality and Chirality Recognition.

■ REFERENCES

(1) Fráter, G. *Helv. Chim. Acta* **1979**, *62*, 2825−2828.

(2) (a) Fráter, G.; Müller, U.; Günther, W. *Tetrahedron* **1984**, *40*, 1269−1277. (b) Seebach, D.; Wasmuth, D. *Helv. Chim. Acta* **1980**, *63*, 197−200.

(3) Khan, A. A.; Chee, S. H.; Stocker, B. L.; Timmer, M. S. M. *Eur. J. Org. Chem.* **2012**, 995−1002.

(4) Ratovelomanana-Vidal, V.; Girard, C.; Touati, R.; Tranchier, J. P.; Hassine, B. B.; Genêt, J. P. *Adv. Synth. Catal.* **2003**, *345*, 261−274.

(5) Nishizawa, M.; Yamamoto, H.; Imagawa, H.; Barbier-Chassefière, V.; Petit, E.; Azuma, I.; Papy-Garcia, D. *J. Org. Chem.* **2007**, *72*, 1627−1633.

(6) Barry, C. E.; Lee, R. E.; Mdluli, K.; Sampson, A. E.; Schroeder, B. G.; Slayden, R. A.; Yuan, Y. *Prog. Lipid Res.* **1998**, *37*, 143−179.

(7) Kaur, D.; Guerin, M. E.; Skovierova, H.; Brennan, P. J.; Jackson, M. *Adv. Appl. Microbiol.* **2009**, *69*, 23−78.

(8) (a) Brotin, T.; Vanthuyne, N.; Cavagnat, D.; Ducasse, L.; Buffeteau, T. *J. Org. Chem.* **2014**, *79*, 6028−6036. (b) Cherblanc, F. L.; Lo, Y.-P.; Herrebout, W. A.; Bultinck, P.; Rzepa, H. S.; Fuchter, M. J. *J. Org. Chem.* **2013**, *78*, 11646−11655. (c) Yang, G.; Li, J.; Liu, Y.; Lowary, T. L.; Xu, Y. *Org. Biomol. Chem.* **2010**, *8*, 3777−3783.

(9) (a) Torres-Valencia, J. M.; Chávez-Ríos, O. E.; Cerda-García-Rojas, C. M.; Burgueño-Tapia, E.; Joseph-Nathan, P. *J. Nat. Prod.* **2008**, *71*, 1956−1960. (b) Muñoz, M. A.; Chamy, C.; Bucio, M. A.; Hernández-Barragán, A.; Joseph-Nathan, P. *Tetrahedron Lett.* **2014**, *55*, 4274−4277.

(10) (a) Polavarapu, P. L. *Chirality* **2008**, *20*, 664−672. (b) Polavarapu, P. L. *Chirality* **2012**, *24*, 909−920.

(11) (a) Hoye, T. R.; Jeffrey, C. S.; Shao, F. *Protocols* **2007**, *10*, 2451−2458. (b) Seco, J. M.; Quiñoá, E.; Riguera, R. *Chem. Rev.* **2004**, *104*, 17−117. (c) Dale, J. A.; Mosher, H. S. *J. Am. Chem. Soc.* **1973**, *95*, 512−519.

(12) Petrovic, A. G.; Bose, P. K.; Polavarapu, P. L. *Carbohydr. Res.* **2004**, *339*, 2713−2720.

(13) Zhang, P.; Polavarapu, P. L. *Appl. Spectrosc.* **2006**, *60*, 378−385.

(14) Shanmugam, G.; Polavarapu, P. L. *J. Am. Chem. Soc.* **2004**, *126*, 10292−10295.

(15) (a) Shanmugam, G.; Polavarapu, P. L. *Biophys. J.* **2004**, *87*, 622−630. (b) Shanmugam, G.; Polavarapu, P. L.; Gopinath, D.; Jayakumar, R. *Biopolym.: Pept. Sci.* **2005**, *80*, 636−642. (c) Shanmugam, G.; Polavarapu, P. L. *Biophys. Chem.* **2004**, *111*, 73−77.

(16) Kurouski, D.; Lombardi, R. A.; Dukor, R. K.; Lednev, I. K.; Nafie, L. A. *Chem. Commun.* **2010**, *46*, 7154−7156.

(17) (a) Petrovic, A. G.; Polavarapu, P. L. *J. Phys. Chem. B* **2005**, *109*, 23698−23705. (b) Shanmugam, G.; Polavarapu, P. L. *Appl. Spectrosc.* **2005**, *59*, 673−681.

(18) Castiglioni, E.; Biscarini, P.; Abbate, S. *Chirality* **2009**, *21*, E28−E36.

(19) (a) Merten, C.; Kowalik, T.; Hartwig, A. *Appl. Spectrosc.* **2008**, *62*, 901−905. (b) Buffeteau, T.; Lagugné-Labarthet, F.; Sourisseau, C. *Appl. Spectrosc.* **2005**, *59*, 732−745.

(20) (a) Dezhahang, Z.; Poopari, M. R.; Xu, Y. *Chem.—Asian J.* **2013**, *8*, 1205−1212. (b) Debie, E.; Jaspers, L.; Bultinck, P.; Herrebout, W.; Van Der Veken, B. *Chem. Phys. Lett.* **2008**, *450*, 426−430.

(21) Losada, M.; Tran, H.; Xu, Y. *J. Chem. Phys.* **2008**, *128*, 014508/1−11.

(22) Yang, G.; Xu, Y. *Phys. Chem. Chem. Phys.* **2008**, *10*, 6787−6795.

(23) Gobi, S.; Vass, E.; Magyarfalvi, G.; Tarczay, G. *Phys. Chem. Chem. Phys.* **2011**, *13*, 13972−13984.

(24) Rablen, P. R.; Pearlman, S. A.; Finkbiner, J. *J. Phys. Chem. A* **1999**, *103*, 7357−7363.

(25) Poopari, M. R.; Dezhahang, Z.; Xu, Y. *Phys. Chem. Chem. Phys.* **2013**, *15*, 1655−1665.

(26) (a) Thomas, J.; Sukhorukov, O.; Jäger, W.; Xu, Y. *Angew. Chem., Int. Ed.* **2014**, *53*, 1156−1159. (b) Thomas, J.; Sukhorukov, O.; Jäger, W.; Xu, Y. *Angew. Chem., Int. Ed.* **2013**, *52*, 4402−4405.

(27) (a) Muñoz, M. A.; Areche, C.; Rovirosa, J.; San-Martín, A.; Joseph-Nathan, P. *Heterocycles* **2010**, *81*, 625−635. Cichewicz, R. H.; Clifford, L. J.; Lassen, P. R.; Cao, X.; Freedman, T. B.; Nafie, L. A.; Deschamps, J. D.; Kenyon, V. A.; Flanary, J. R.; Holman, T. R.; Crews, P. *Bioorg. Med. Chem.* **2005**, *13*, 5600−5612.

(28) Dennington, R.; Keith, T.; Millam, J. *GaussView*, Version 5; Semichem Inc.: Shawnee Mission, KS, 2009.

(29) (a) Frelek, J.; Butkiewicz, A.; Gorecki, M.; Wojcieszczyk, R. K.; Luboradzki, R.; Kwit, M.; Rodee, M. F.; Szczepek, W. J. *RSC Adv.* **2014**, *4*, 43977−43993. (b) Bouchet, A.; Brotin, T.; Linares, M.; Ågren, H.; Cavagnat, D.; Buffeteau, T. *J. Org. Chem.* **2011**, *76*, 1372−1383.

(30) (a) Dezhahang, D.; Poopari, M. R.; Hernández, F. E.; Diaz, C.; Xu, Y. *Phys. Chem. Chem. Phys.* **2014**, *16*, 12959−12967. (b) Losada, M.; Xu, Y. *Phys. Chem. Chem. Phys.* **2007**, *9*, 3127−3135.

(31) Harada, N.; Nakanishi, K. *Circular Dichroic Spectroscopy Exciton Coupling in Organic Stereochemistry*; University Science Books: Mill Valley, CA, 1983.

(32) Taniguchi, T.; Monde, K. *J. Am. Chem. Soc.* **2012**, *134*, 3695−3698.

(33) Berova, N.; Nakanishi, K.; *Circular Dichroism: Principles and Applications*, 2nd ed.; Berova, N., Nakanishi, K., Woody, R. W., Eds.; Wiley-VCH: New York, 2000; p 337.

(34) (a) Williams, S. D.; Johnson, T. J.; Sharpe, S. W.; Yavelak, V.; Oates, R. P.; Brauer, C. S. *J. Quant. Spectrosc. Radiat. Transfer* **2013**, *129*, 298−307. (b) Luttschwager, N. O. B.; Wassermann, T. N.; Mata, R. A.; Suhm, M. A. *Angew. Chem., Int. Ed.* **2012**, *52*, 463−466. (c) Wexler, A. S. *Spectrochim. Acta* **1965**, *21*, 1725−1742.

(35) Roy, D.; Marianski, M.; Maitra, N. T.; Dannenberg, J. J. *J. Chem. Phys.* **2012**, *137*, 134109/1−12.

(36) Frisch, M. J.; Trucks, G. W.; Schlegel, H. B.; Scuseria, G. E.; Robb, M. A.; Cheeseman, J. R.; Scalmani, G.; Barone, V.; Mennucci, B.; Petersson, G. A.; Nakatsuji, H.; Caricato, M.; Li, X.; Hratchian, H.

P.; Izmaylov, A. F.; Bloino, J.; Zheng, G.; Sonnenberg, J. L.; Hada, M.; Ehara, M.; Toyota, K.; Fukuda, R.; Hasegawa, J.; Ishida, M.; Nakajima, T.; Honda, Y.; Kitao, O.; Nakai, H.; Vreven, T.; Montgomery, J. A., Jr.; Peralta, J. E.; Ogliaro, F.; Bearpark, M.; Heyd, J. J.; Brothers, E.; Kudin, K. N.; Staroverov, V. N.; Kobayashi, R.; Normand, J.; Raghavachari, K.; Rendell, A.; Burant, J. C.; Iyengar, S. S.; Tomasi, J.; Cossi, M.; Rega, N.; Millam, N. J.; Klene, M.; Knox, J. E.; Cross, J. B.; Bakken, V.; Adamo, C.; Jaramillo, J.; Gomperts, R.; Stratmann, R. E.; Yazyev, O.; Austin, A. J.; Cammi, R.; Pomelli, C.; Ochterski, J. W.; Martin, R. L.; Morokuma, K.; Zakrzewski, V. G.; Voth, G. A.; Salvador, P.; Dannenberg, J. J.; Dapprich, S.; Daniels, A. D.; Farkas, Ö.; Foresman, J. B.; Ortiz, J. V.; Cioslowski, J.; Fox, D. J. *Gaussian 09*, Revision C.01; Gaussian, Inc.: Wallingford, CT, 2009.

(37) Kohn, W.; Sham, L. J. *Phys. Rev.* **1965**, *140*, A1133−A38.

(38) (a) Becke, A. D. *J. Chem. Phys.* **1993**, *98*, 5648−5652. (b) Lee, C. T.; Yang, W. T.; Parr, R. G. *Phys. Rev. B: Condens. Matter Mater. Phys.* **1988**, *37*, 785−789.

(39) Kendall, R. A.; Dunning, T. H., Jr.; Harrison, R. J. *J. Chem. Phys.* **1992**, *96*, 6796−6806.

(40) Nafie, L. A. *Vibrational Optical Activity: Principles and Applications*; John Wiley & Sons Ltd.: New York, 2011.

(41) *SPARTAN '08*; Wavefunction, Inc.: Irvine, CA, 2008; www.wavefun.com/products/spartan.html.

(42) Dewar, M. J. S.; Zoebisch, E. G.; Healy, E. F. *J. Am. Chem. Soc.* **1985**, *107*, 3902−3909.